THE OPTICAL ABSORPTION OF THE NEUTRAL VACANCY IN DIAMOND

M. LANNOO

Institut Supérieur d'Electronique du Nord, Lille, France

and

A. M. STONEHAM

Theoretical Physics Division, AERE Harwell, Berkshire, U.K.

Abstract — Optical absorption by the neutral vacancy in diamond has been predicted to occur between the ground ^1E state and the $^1T_2$ excited state. Both these states are orbitally degenerate and should show Jahn Teller distortions. We have calculated the Huang–Rhys Factor for the transition (the fraction of the intensity in the zero phonon line) and the first and second moments of the absorption band. Also we discuss the response of the zero phonon line to externally applied stresses. Our model assumes that the vacancy interacts with just six modes, corresponding to the normal modes of the neighbours of the vacancy. The coupling of the electronic and nuclear motion is estimated from an LCAO model.

The results are compared with observations of the GR1 band, which has been attributed to the vacancy. The predicted Huang–Rhys factor $S \sim 3\cdot7$ and the first and second moments of the band support this identification. Further our model predicts that luminescence from this band should be unpolarised, as observed. However the predicted stress splitting of the zero phonon line differs from that observed. Possible explanations of this are discussed.

1. INTRODUCTION

THE PRIMARY defects in diamond — such as the vacancy and the interstitial — have still to be identified with any certainty. The optical GR1 band has been suggested as arising from the neutral vacancy, V^0, although other models have been proposed. Theoretically work has concentrated on energies of formation [1, 2], on the positions of the bands associated with the primary defects [3–6] and on the existence and magnitude of the Jahn–Teller effect [7–9]. Here we concentrate on the form of the band arising from the neutral vacancy.

The various treatments of the vacancy [3, 4, 6] are generally in qualitative agreement on the low lying levels. Only excited states should give spin resonance, and the optical transition energy is less than one would predict on a one-electron model. It is hard to devise means of distinguishing the vacancy and interstitial [5] for the structure of the low lying energy levels is predicted to be similar,

and it is difficult to make accurate calculations of the transition energies. This difficulty is enhanced by the existence of the Jahn–Teller effect, although it probably affects the shapes of the optical bonds more severely than the transition energies.

The form of the absorption band is measured by the Huang–Rhys Factor, S, which gives a measure of the fractional intensity in the zero phonon line, the Stokes shift and the bandwidth [10–13]. When S is small, as for the GR1 band, a sharp zero phonon line should be seen. For centres with large S, such as F centres in alkali halides, only a broad, nearly Gaussian, line is seen. The Huang–Rhys factor appropriate to the GR1 band has been measured experimentally [14–16]. We calculate the Huang–Rhys factor for the neutral vacancy (Section 4) and compare our predictions with these measurements on the GR1 band.

Closely related calculations (Section 5) predict the shift of a zero phonon line under

external uniaxial stress. Experimentally the uniaxial stress method is a very sensitive way of determining the symmetry of a centre. The method has been used by Runciman[17] and Crowther[18] on the GR1 system, and our results for the vacancy are compared with their data.

The calculations described here refer only to the neutral vacancy. It is necessary to ask if the centre giving rise to the GR1 band and the vacancy are identical. In Section 6, where we compare our calculations with experiment, we find the Huang–Rhys factor suggests the two centres are the same. The stress splitting data is also consistent with the identification, but only if the Jahn–Teller effect is important in a rather complicated way. One simple conclusion is possible: if the data are qualitatively inconsistent with the GR1 centre being the vacancy then they are also inconsistent with it being the neutral interstitial. This can be seen very easily by recalling that the relevant low lying energy levels are the same in both cases. Figure 1 compares them.

2. THE STATIC JAHN–TELLER EFFECT

The optical transition of lowest energy for the neutral vacancy is believed to be from a ^1E state to a $^1T_2$ excited state[3, 4]. Both these states have electronic degeneracy, so that the Jahn–Teller theorem requires that they distort, with a corresponding lowering of energy.

We assume that only the nearest neighbours of the vacancy contribute to its interaction with lattice distortions. As the vacancy wave function is reasonably compact and there are no long range electrostatic interactions this may be quite a good assumption. There are four neighbours, so their configuration can be described by twelve normal coordinates. Three are rotations and three translations; these we ignore. The remaining six are the A_1 mode, Q_a, the E modes Q_ϵ and Q_θ, and the T_2 modes Q_ξ, Q_η and Q_ζ. The Q_a mode is the 'breathing' mode in which all the neighbours move symmetrically. The E modes correspond to tetragonal distortions; under T_dQ_θ trans-
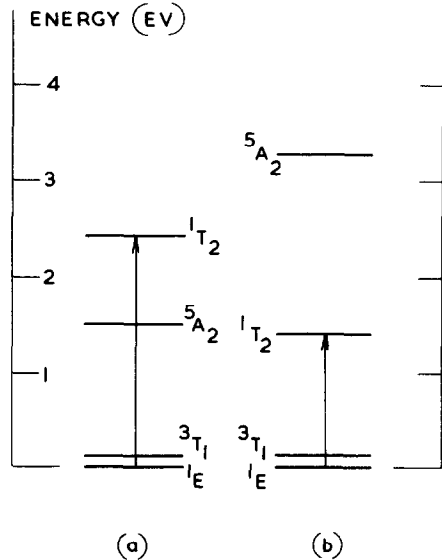

Fig. 1. Energy levels of the neutral vacancy and interstitial in diamond. (a) The neutral vacancy[1], and (b) the neutral interstitial[3].

forms like $2x^2 - y^2 - z^2$ and Q_ϵ like $y^2 - z^2$. The T_2 modes describe trigonal distortions. Exact definitions of the modes in terms of the displacements are given in the Appendix.

The ^1E electronic state comprises two states, $|\epsilon>$ and $|\theta>$, degenerate in the undistorted environment when the electronic energy is E_g. The vibronic Hamiltonian in the ^1E manifold can be written:

$$\mathcal{H}_g = \left[E_g + \sum_\alpha \left\{ -\frac{\hbar^2}{2M} \frac{\partial^2}{\partial Q_\alpha^2} \right.\right.$$

$$\left.\left. + \tfrac{1}{2} M \omega_\alpha^2 Q_\alpha^2 \right\} \right] \begin{pmatrix} 1 & 0 \\ 0 & 1 \end{pmatrix}$$

$$+ I_{gE} Q_\epsilon \begin{pmatrix} -1 & 0 \\ 0 & 1 \end{pmatrix} + I_{gE} Q_\epsilon \begin{pmatrix} 0 & 1 \\ 1 & 0 \end{pmatrix}. \quad (2.1)$$

The two dimensional form is because ^1E is doubly degenerate. The first term gives the electronic energy for zero Q_α, the nuclear kinetic energy and the elastic energy. M is the mass of one Carbon atom and ω_α is the 'effective frequency' for mode α; these frequencies are discussed in more detail in

the next section. The terms proportional to I_{gE} give rise to the Jahn–Teller effect, and it is easily shown from (2.1) that Q_θ and Q_ϵ oscillate about $Q_{g\theta}$ and $Q_{g\epsilon}$ where

$$Q_{g\theta}^2 + Q_{g\epsilon}^2 = \{I_{gE}/(M\omega_E^2)\}^2. \qquad (2.2)$$

In the absence of the Jahn–Teller term all the coordinates oscillate about their zero values. When I_{gE} is finite the degeneracy of $|\epsilon\rangle$ and $|\theta\rangle$ is lifted, and the ground state energy reduced by

$$\Delta E_{gE} = I_{gE}^2/2M\omega_E^2. \qquad (2.3)$$

The new equilibrium configuration is not determined completely by (2.2), which only relates $Q_{g\epsilon}$ and $Q_{g\theta}$. This ambiguity is a result of the simple Hamiltonian (2.1), and its neglect of higher order terms. These higher terms fix both $Q_{g\theta}/Q_{g\epsilon}$ and the sign of $Q_{g\theta}$. The relative values of $Q_{g\epsilon}$ and $Q_{g\theta}$ are determined by the crystal symmetry—in a cubic crystal one expects tetragonal rather than orthorhombic distortions. For a tetragonal distortion along the x axis $Q_{g\epsilon} = 0$, so

$$|Q_{g\theta}| = |I_{gE}|/(M\omega_E^2). \qquad (2.4)$$

Equivalent results hold for y and z tetragonal distortions. The sign of $Q_{g\theta}$ for the x distortion can only be fixed by detailed knowledge of the higher order terms. We work with both possibilities throughout. Later we find that $Q_{g\theta} < 0$ ($|\epsilon\rangle$ ground state for an x tetragonal distortion) is more consistent with the stress splitting data for the GR1 band. In some ways this is surprising, for $Q_{g\theta} > 0$ causes the neighbours of the vacancy to move together in pairs. As there is a strong tendency to form pairwise bonds, one might expect $Q_{g\theta} > 0$ to be favoured by enhanced bonding[1].

The $^1T_2$ state comprises three electronic states $|\xi\rangle|\eta\rangle$ and $|\zeta\rangle$, degenerate when all the Q_α are zero. We will assume that the equilibrium values of Q_a, the breathing mode, are identical in the ^1E and $^1T_2$ states. This assumption is made because ^1E and $^1T_2$ are both derived from the same electronic con-

figuration. Such as assumption would of course, be quite inappropriate for the F centre in alkali halides, where the initial and final states derive from different configurations. The vibronic Hamiltonian for the $^1T_2$ state is more complicated than (2.1) because there are terms linear in all five remaining coordinates. In the following expression we assume that the effective frequencies, ω_α, are the same as in the ground state Hamiltonian. Again this should be reasonable because the two electronic states derive from the same configuration.

$$\mathscr{H}_e = \left[E_e + \sum_\alpha \left\{ -\frac{\hbar^2}{2M} \frac{\partial^2}{\partial Q_\alpha^2} + \tfrac{1}{2}M\omega_\alpha^2 Q_\alpha^2 \right\} \right]$$

$$\begin{pmatrix} 1 & 0 & 0 \\ 0 & 1 & 0 \\ 0 & 0 & 1 \end{pmatrix}$$

$$+ I_{eE} \begin{pmatrix} 2Q_\theta & \cdot & \cdot \\ \cdot & -Q_\theta + \sqrt{3}\,Q_\epsilon & \cdot \\ \cdot & \cdot & -Q_\theta - \sqrt{3}\,Q_\epsilon \end{pmatrix}$$

$$+ I_{eT} \begin{pmatrix} \cdot & Q_\zeta & Q_\eta \\ Q_\zeta & \cdot & Q_\xi \\ Q_\zeta & Q_\xi & \cdot \end{pmatrix}. \qquad (2.5)$$

The terms in I_{eE} and I_{eT} are responsible for the Jahn–Teller effect. With this vibronic Hamiltonian one of two different types of distorted configuration can give a minimum in the energy. If the stable configuration is tetragonally distorted the energy reduction is

$$\Delta E_{eE} = 4 \frac{I_{eE}^2}{2M\,\omega_E^2}. \qquad (2.6)$$

Alternatively if trigonal distortions give the stable configuration

$$\Delta E_{eT} = \frac{4}{3} \frac{I_{eT}^2}{2M\,\omega_T^2}.$$

The trigonal distortion is stable if ΔE_{eT} exceeds ΔE_{eE}. In the present case these two energies are similar in magnitude, and the relative values of ω_E and ω_T are important.

Our conclusion (§3) that $\omega_E = \sqrt{2}\omega_T$ leads to a *trigonal* minimum, using the data in Table 1. Thus we predict a tetragonally distorted ^1E ground state and a trigonally distorted $^1T_2$ excited state. The difference in symmetry in the two cases combined with the degeneracy of both the ground and excited states makes the present problem rather complex.

Table 1

$I_{gE} = 2.04$ eV/a.u.	$\Delta E_{gE} = 0.09$ eV
$I_{eE} = 1.59$ eV/a.u.	$\Delta E_{eE} = 0.23$ eV
$I_{eT} = 2.54$ eV/a.u.	$\Delta E_{eT} = 0.39$ eV

The values of I_{gE}, I_{eE} and I_{eT} given in Table 1 have been calculated using an LCAO model for the vacancy, In this model[9] the atomic orbitals from which the defect electron wave functions are constructed move rigidly with the nuclei with which they are associated. All calculations of Jahn–Teller integrals introduce approximations, so these results are best considered as order of magnitude estimates. In principle these integrals can be found from experimental uniaxial stress data. This is discussed in Section 5.

3. THE LATTICE SYSTEM

The effective frequencies ω_E and ω_T were introduced in equations (2.1) and (2.5) to describe the elastic energy associated with distortions of the environment of the vacancy. These terms in ω_E and ω_T limit the Jahn–Teller distortion.

There are two important frequencies in our problem — one for E modes and one for T modes. One of the most severe approximations in this calculation is the assumption that we can use a small number of discrete frequencies instead of a distribution of frequencies. The ratio of ω_E and ω_T can be calculated on a simple model. In this the neighbours of the vacancy are the only atoms allowed to move, the rest of the lattice remaining fixed. If the atoms interact by nearest neighbour central forces then[8]

$$\omega_E = \sqrt{2}\,\omega_T. \qquad (3.1)$$

The assumption that only the neighbours move is very primitive, although it is qualitatively consistent with the assumption that only these neighbours contribute to the electron–phonon interaction. The conclusion that $\omega_E > \omega_T$ can, however, be seen rather easily. In creating the vacancy several bonds were broken. These bonds contributed more to the elastic energy in T distortions than in the E moles.

In choosing a value for ω_E we assume, rather arbitrarily, that it is equal to the Raman frequency. This is because the density of vibrational states in diamond is peaked near this energy, which forms an upper bound to the phonon energies in the perfect lattice. With equation (3.1) we find

$$\hbar\omega_E = 0.165 \text{ eV}; \quad \hbar\omega_T = 0.095 \text{ eV}. \qquad (3.2)$$

In fact ω_T lies very close to the effective phonon energies for the GR1 band which is sometimes associated with the neutral vacancy. As we will find the T_2 modes most important this is encouraging. In fact the one phonon part of the GR1 band has a peak at 0.040 eV, so it is clear that phonons over a range of energies are important. This particular peak is very stress sensitive[18] suggesting a localised resonant mode.

With these figures for the lattice frequencies we obtain the energy lowerings due to the Jahn–Teller effect from equations (2.3), (2.6) and (2.7). These are shown in Table 1. The trigonal distortions are favoured in the excited state by a fairly small margin. In the ground state the distortion amplitude is $|Q_{g\theta}| = 0.05$ A from (2.4).

There is some doubt as to whether the Jahn–Teller effect is static or dynamic. The basic question is the ease of tunnelling between equivalent distortions of the environment. In this article we will consider the static case in detail (no tunnelling) although we will mention the qualitative effects peculiar to

the dynamic case. The possibility of dynamic effects can be seen by noting ΔE_{gE} is only 0·09 eV ($\equiv$k. 1100°) and must equal or exceed the barrier for reorientation. The GR1 system, sometimes attributed to the vacancy, is visible up to 900°K, although the zero phonon line is not visible above about 400°K. Rapid tunnelling (the dynamic effect) should show more readily on the zero phonon line. Further calculations are in progress on this point.

We are also interested in the vibronic Hamiltonian near to the absolute minima in the distorted configurations. When there is no Jahn–Teller effect there is only one minimum, at $Q = 0$. The energy surfaces are determined by the elastic energy, of the form:

$$\tfrac{1}{2}M[\omega_E^2(Q_\theta^2 + Q_\epsilon^2) + \omega_T^2(Q_\xi^2 + Q_\eta^2 + Q_\zeta^2)].$$

The Jahn–Teller effect in the ground state leads to three equivalent minima, corresponding to the three possible tetragonal distortions. Near each minimum the energy surface has a modified form. Thus for the tetragonal minimum at $(Q_\theta, Q_\epsilon) = (Q_{g\theta}, 0)$ we have instead

$$\tfrac{1}{2}M[\omega_E^2(Q_\theta - Q_{g\theta})^2 + \bar{\omega}_E^2 Q_\epsilon^2 + \omega_T^2(Q_\xi^2 + Q_\eta^2 + Q_\zeta^2)]$$

The second frequency, $\bar{\omega}_E$, is related to ω_E, to the energy barrier between the tetragonal distortions along different axes, and to the Jahn–Teller energy ΔE_{gE}. Qualitatively the important features are shown by the results for low barriers:

$$\bar{\omega}_E = \omega_E^{\frac{3}{2}} \sqrt{(B/\Delta E_{gE})}.$$

Our choice of $\bar{\omega}_E$ is not too important, for the corresponding coordinate, Q_ϵ, has the same value in the ground and excited state minima. Whenever $\bar{\omega}_E$ occurs we assume it equal to ω_E, mainly for simplicity. The assumption does imply that the barrier, B, is fairly high, consistent with our assumption of a static

Jahn–Teller effect. Such a high barrier may be reasonable for a system like diamond where there are strong directional bonds between atoms.

4. THE HUANG–RHYS FACTOR AND THE MOMENTS OF THE LINE

4.1 Introduction

The Huang–Rhys factor, S, is a dimensionless parameter which determines the qualitative features of optical absorption and emission lines [9–11]. It is still a useful parameter beyond the particular model in which it was introduced, as it is related to the fractional intensity of the zero phonon line and to the mean number of phonons emitted in an optical transition. In this section we will calculate the first three moments of the whole resonance line and the fraction of its intensity in the zero phonon line. The predictions will be compared with experiment in Section 6. Throughout we assume the temperature is absolute zero.

To establish our notation we discuss the system shown in Fig. 2. This simple example considers a transition between two non-degenerate states interacting strongly with just one phonon mode, Q. The transition $A \rightarrow B$ in Fig. 2. is the Frank–Condon transition, in which the nuclear configuration does not change. The zero phonon transition is $A \rightarrow C$, in which the phonon occupation number is unaltered. Transitions in which the occupation number is changed by 1,2,3... are allowed, and give rise to a broad band.

Fig. 2. Configuration coordinate diagram of a simple system with non-degenerate levels interacting with one mode Q.

The Huang–Rhys factor, S_0, is related to the fractional intensity, F, in the zero phonon line by

$$S_0 = -\ln F. \qquad (4.1)$$

We adopt this definition for both the simple system and for the vacancy, the subscript O is used to distinguish it from other possible definitions mentioned later.

The zeroth moment of the line, M_0, is a measure of the integrated intensity, and is taken to be

$$M_0 = Av \sum_e |<e|\,\Omega\,|g>|^2. \qquad (4.2)$$

The higher moments are defined by[11, 12]:

$$\hbar^n M_n = \frac{Av \sum_e |<e|\Omega|g>|^2 \{E_e - E_g - h\nu\}^n}{Av \sum_e |<e|\Omega|g>|^2} \qquad (4.3)$$

for $n \geq 1$. In these expressions $|g>$ is the ground state, $|e>$ an excited state, and Ω is the dipole operator inducing the transition. The photon energy is $h\nu$, and the average is over the vibrational wave function in the ground state.

In our simple example the first moment of the line is related to the Stokes shift $(E_B - E_C)$:

$$\hbar M_1 = E_B - E_C \qquad (4.4)$$

and the second moment to the width, H_0, of the band:

$$\hbar^2 M_2 = H_0^2/8 \ln 2. \qquad (4.5)$$

In more complicated situations there are no simple relations like these, and calculated moments should be compared directly with measured moments. Unfortunately it is often hard to measure moments, because of uncertainties in the background intensity. Theoretically the calculation of the detailed line shape is only possible in very simple models, and for this reason we resort to moments.

It is possible to introduce other definitions of the Huang–Rhys factor through (4.4) and (4.5) viz $S \equiv M_1/\omega$ and $S_2 \equiv M_2/\omega^2$ (M_2 is the second moment about the centroid of the band). For simple systems $S_0 \sim S_1 \sim S_2$. We will find, however, that analogous defi-nitions for complex systems give widely different values for S_0, S_1 and S_2.

4.2 Vibronic wave functions

We now consider the vacancy, where, in our simple model, both initial and final states are degenerate and interact with six modes. The vibronic (vibrational plus electronic) wave function for the system must be specified further. The important effect of electronic degeneracy is that the simple Born–Oppenheimer approximation does not apply. It is no longer possible to factorise the vibronic wave function $\Psi(q,Q)$ into a vibrational part $\chi(Q)$ and an electronic part $\phi(q,Q)$. In these functions q represents the defect electron coordinates and Q the set of normal coordinates describing distortions of the vacancy environment. If there are N such normal coordinates and the electronic level has degeneracy D then the vibronic functions are usually well described by a linear combination of ND terms each of the form $\chi(Q)\phi(q,Q)$. In some special cases the vibronic wave function has a particularly simple form. One such case occurs in the calculation of the intensity of the zero phonon line. The states involved in the zero phonon transitions are, loosely speaking, those with the minimum energy configurations in the initial and final states. Near each minimum we may use an approximate vibronic function similar to the Born–Opperheimer form. If the minimum is at $Q_\alpha \equiv Q_{\alpha m}$ when the electronic state is $|m>$ then the lowest vibronic function near the minimum is

$$\Psi_m \simeq |m> \prod_{\alpha=1}^n \chi_\alpha (Q_\alpha - Q_{\alpha m}). \qquad (4.6)$$

χ_α is the lowest harmonic-oscillator wave function for mode α. This approximation should be acceptable for distortions Q such that the different sheets of the vibrational energy surface are well separated[19, 20].

Later we calculate the moments M_0, M_1 and M_2 using expressions (4.2) and (4.3). The system is initially in state $|g>$ which is the ground electronic state and the lowest

vibrational state. The arguments leading to (4.6) allow us to write

$$|g> = |ge>|\tilde{g}\mu>$$

for each of the equivalent Jahn–Teller distorted states; $|ge>$ is purely electronic, and $|\tilde{g}\mu>$ is a vibrational function. We assume $|ge>$ is not sensitive to Q in the neighbourhood of the ground state minimum. The averages in (4.2) and (4.3) now include averaging over the differently oriented distortions in the ground state.

Excited state functions of the form (4.6) can only be used in calculating the zero phonon line intensity. When we calculate the moments of the whole band the vibronic wave functions well away from the minima are needed. In general we have

$$|e> = \sum_{j,m} a_{e;jm}|je>|\tilde{jm}>$$

where the $|je>$ are the degenerate electronic functions for the undistorted configuration. $|\tilde{jm}>$ is a vibrational function in which m (like μ in $|\tilde{g}\mu>$) is a label, rather than an occupation number.

4.3 Matrix elements of the dipole operator

The dipole operator connects the electronic states $|ge>$ and $|je>$. Defining

$$\mu_{gj} = <ge|\Omega|je>$$

where Ω is the dipole operator, we may find the relative values of the μ_{gj} by symmetry arguments. If the electric field vector has direction cosines (α, β, γ) and the three T_2 states are labelled $|x>,|y>,|z>$, then

$$\mu_{\theta x}: \mu_{\theta y}: \mu_{\theta z} = 2\alpha : -\beta : -\gamma$$

$$\mu_{\epsilon x}: \mu_{\epsilon y}: \mu_{\epsilon z} = 0 : \sqrt{3}\beta : -\sqrt{3}\gamma.$$

If we define the proportionality constant by $\mu_{\theta x} \equiv 2\alpha K$ then the zeroth moment is, by (4.2)

$$M_{0\epsilon} = M_{0\theta} = 2K^2. \qquad (4.7)$$

The suffices ϵ, θ refer to the two possible electronic ground states mentioned in section 2.

4.4 Calculation of the Huang–Rhys factor and moments

We can now calculate S_0 from the fractional intensity in the zero phonon line. This is done explicitly for the $|\theta>$ ground state. Near the minimum energy configuration in the ground state the lowest vibronic function is (by (4.6))

$$\Psi_{g\theta} \simeq |\theta> \prod_\alpha \chi_\alpha(Q_\alpha - Q_{\alpha g}).$$

Similarly near the (111) minimum in the excited state

$$\Psi_e^{111} \simeq \frac{1}{\sqrt{3}}(|x> + |y> + |z>)\prod_\alpha$$
$$\cdot \chi_\alpha(Q_\alpha - Q_{\alpha e})$$

with corresponding equations for the other minima. The matrix elements of Ω connecting these states are products of μ_{gj} elements and vibrational overlap integrals:

$$\int dQ_\alpha \chi_\alpha(Q_\alpha - Q_{\alpha g})\chi_\alpha(Q_\alpha - Q_{\alpha e})$$
$$= \exp\left\{-\frac{M\omega_\alpha}{2\hbar}(Q_{\alpha g} - Q_{\alpha e})^2\right\}.$$

The fractional intensity in the zero phonon line is then

$$F = \frac{1}{M_0}Av\sum_P |<\Psi_{g\theta}|\Omega|\Psi_e^P>|^2.$$

As in (4.1) we have $S_0 \equiv -\ln F$; after simplification

$$S_{0\epsilon} = S_{0\theta} = \frac{I_{gE}^2}{2M\hbar\omega_E^3} + \frac{2}{3}\frac{I_{eT}^2}{M\hbar\omega_T^3} - \ln\left(\frac{4}{3}\right). \qquad (4.8)$$

The result for an $|\epsilon>$ ground state is also given in (4.8).

The higher moments of the absorption line

can be simplified by writing them in terms of averages:

$$\langle \mathbf{A} \rangle = \frac{Av \sum\limits_{j,k} \mu_{gi} \mu_{kg} A_{jk}}{M_0}. \qquad (4.9)$$

The average Av is over the vibrational parts of the ground state wave functions, and it also includes averaging over the alternative tetragonally-distorted ground states. The vibrational average must be performed with caution, for the mean values of Q_θ and Q_ϵ are affected by the static Jahn–Teller effect. Thus for vacancies with a static distortion $Q_{g\theta}$ we have

$$Av(Q_\theta) = Q_{g\theta}$$

and, for all α or β, at $0°K$

$$Av\{(Q_\alpha - Q_{g\alpha})^2\} = \hbar/2M\omega_\alpha$$
$$Av(Q_\alpha Q_\beta) = 0 \quad \text{if } \alpha \neq \beta.$$

The averages in (4.9) differ from those of [10], where the calculation is slightly oversimplified and the μ factors omitted. Our averages agree with those of Henry, Schnatterly and Slichter[23]. The μ factors have a significant effect in the calculation.

The Stokes shift is found from the transition energy of the zero phonon line:

$$E_{zpl} = h\nu_0 + \Delta E_{gE} - \Delta E_{eT},$$

in which $h\nu_0$ is the transition energy for $Q = 0$, and from the centroid of the band at

$$\bar{E} = \hbar\nu_0 + \langle \Lambda \rangle - \langle \Gamma \rangle. \qquad (4.10)$$

The Λ operator consists of the electron-phonon terms in (2.5), viz

$$\Lambda = I_{eE} \begin{pmatrix} 2Q_\theta & \cdot & \cdot \\ \cdot & -Q_\theta + \sqrt{3}\,Q_\epsilon & \cdot \\ \cdot & \cdot & -Q_\theta - \sqrt{3}Q_\epsilon \end{pmatrix}$$
$$+ I_{eT} \begin{pmatrix} \cdot & Q_\zeta & Q_\eta \\ Q_\zeta & \cdot & Q_\xi \\ Q_\eta & Q_\xi & \cdot \end{pmatrix}.$$

The Γ operator gives the Jahn–Teller terms in the ground state. Thus for the $|\theta\rangle$ state which distorts in the X direction $\Gamma = -I_{g\theta} Q_\theta \delta_{ij}$. Direct evaluation of (4.10) shows that M_1, measured with respect to the zero phonon line, is given by

$$\hbar M_{1\epsilon} = \hbar M_{1\theta} = \frac{I_{gE}^2}{2M\omega_E^2} + \frac{I_{gE} I_{eE}}{M\omega_E^2} + \frac{2}{3}\frac{I_{eT}^2}{M\omega_T^2}. \qquad (4.11)$$

The second moment can be found similarly. Thus

$$\hbar^2 M_2 = \{\langle \Lambda^2 \rangle - \langle \Lambda \rangle^2\} + \{\langle \Gamma^2 \rangle - \langle \Gamma \rangle^2\}$$
$$- 2\{\langle \Gamma\Lambda \rangle - \langle \Gamma \rangle \langle \Lambda \rangle\}.$$

This moment is related to the width of the line. After simplification

$$\hbar^2 M_{2\epsilon} = (\hbar\omega_E)^2 \left[\frac{2I_{eE}^2}{M\hbar\omega_E^3} + \frac{I_{gE}^2}{2M\hbar\omega_E^3} + \frac{I_{eE} I_{gE}}{M\hbar\omega_E^3} \right]$$
$$+ (\hbar\omega_T)^2 \frac{I_{eT}^2}{M\hbar\omega_T^3}$$

$$\hbar^2 M_{2\theta} = \hbar^2 M_{2\epsilon} + (\hbar\omega_E)^2 \cdot 2\left(\frac{I_{eE} I_{gE}}{M\hbar\omega_E^3}\right)^2. \qquad (4.12)$$

The second moment is higher for a $|\theta\rangle$ ground state; the first two moments (M_0 and M_1) were the same for both $|\theta\rangle$ and $|\epsilon\rangle$ states. As shown by Gold and Kiel[22] the contributions of the uncoupled E and T modes to the first three moments of the line are additive.

In Table 2 we give the values of S_0, $\hbar M_1$ and $\sqrt{(\hbar^2 M_2)}$. Care is needed in comparison with experiment as it is usual to measure band widths and peak positions rather than the moments. Moments are often hard to measure due to noise and overlap with other transitions; the experimental figures quoted in Table 2 are underestimates. The A_1 modes have been ignored throughout; we estimate they contribute 0·1–0·15 to S_0. The trigonal modes dominate in S_0, so the effective phonon energy should be of order $\hbar\omega_T \sim 0\cdot095$ eV.

We can also calculate S_1 and S_2 from M_1 and M_2 by dividing the E terms by $\hbar\omega_E$ or $(\hbar\omega_E)^2$ and T terms by $\hbar\omega_T$ or $(\hbar\omega_T)^2$ as appropriate. S_1 and S_2 are dimensionless factors like the Huang–Rhys Factor, and are identical to S_0 for the simple system we described earlier. For the vacancy we find $S_0 \approx 3\cdot7$, $S_1 \sim 5\cdot7$ and $S_2 \sim 9\cdot2$, so these three factors are very different.

5. SPLITTING OF THE ZERO PHONON LINE UNDER UNIAXIAL STRESS.

The integrals I_{eE}, I_{eT}, and I_{gE} which occur in the Huang–Rhys factor can be measured by observing the effect of uniaxial stress on the zero phonon line. The way in which the zero phonon line shifts and splits under stress, and the additional information given by the use of polarised light, can also be used to determine the symmetry of the centre giving the zero phonon line.

Loosely speaking, the zero phonon line corresponds to a transition from the minimum of energy for the ground state to a minimum in the excited state. Thus we need to know how these minima move under stress to new configurations $\{Q_\alpha\}$ and the corresponding changes in energy of the minima. The minima for the unstressed crystal were found by seeking the configuration $\{Q_{\alpha0}\}$ which minimised the eigenvalues of (2.1) for the ground state, or (2.5) for the excited state. The procedure is exactly the same for a stressed crystal except that we add the work done by the applied stress

$$\mathcal{H}_S = \sum_\alpha F_\alpha Q_\alpha \hat{1} \qquad (5.1)$$

before minimising. Here F_α is the (constant) stress associated with the strain Q_α and $\hat{1}$ is the unit matrix. The F_α are different for different modes, and depend on the direction of the uniaxial stress. They also depend on the changes in elastic constant near a vacancy. To find them we note that a uniaxial stress σ would produce a configuration in which the Q_α have certain specific values, $Q_\alpha(\sigma)$, in a perfect crystal without a vacancy. With given effective frequencies (essentially the same as given force constants) a particular set of F_α would give a configuration $Q_\alpha(F_\alpha)$ in which $Q_\alpha(F_\alpha)$ is proportional to F_α.

Table 2

		Theory	Experiment
S_0		3·68	3·57
$\hbar M_1$	eV	0·57	$\gtrsim 0\cdot36$ (0·33†)
$(\hbar^2 M_{2\epsilon})^{1/2}$ eV		0·33 ⎱	$\gtrsim 0\cdot22$ (0·19‡)
$(\hbar^2 M_{2\theta})^{1/2}$ eV		0·39 ⎰	

†ΔE_1 of Fig. 4.
‡$\Delta E_2/2\cdot36$ of Fig. 4; for a Gaussian $(\hbar M_2)^{1/2} = \Delta E_2/2\cdot36$.

We simply equate

$$Q_\alpha(F_\alpha) = Q_\alpha(\sigma) \qquad (5.2)$$

for each α and solve for F_α as a function of σ. This, of course, ignores the effect of changes in elastic constant near the vacancy; without rather formidable calculations it can only be hoped that the approximation is not bad. The values of $Q_\alpha(\sigma)$ for various stress directions are given in Table 3; other values can be found by symmetry.

The effects of uniaxial stress can best be seen by example. First we consider a trigonal (111) stress. The vacancies in trigonally distorted excited states are no longer equivalent; the (111) systems will be affected differently from those with $(1\bar{1}\bar{1})$, $(\bar{1},1,\bar{1})$ or $(\bar{1}11)$ distortions. The zero phonon line will be split, and the minima will move in $\{Q_\alpha\}$ space. Figure 3a shows the motion of the excited state minima in $Q_\xi, Q_\eta, Q_\zeta\}$ space. Under the same trigonal stress the three ground state minima, with their x,y and z tetragonal distortions, are not split; they are all symmetrical so far as the trigonal stress is concerned. Figure 3(b) shows the motion of the ground state minima in $\{Q_\theta, \frac{1}{2}[-Q_\theta+\sqrt{3}Q_\epsilon], \frac{1}{2}[-Q_\theta-\sqrt{3}Q_\epsilon]\}$ space.

Secondly we consider a tetragonal (100) stress. The excited state minima are equivalent and so remain degenerate. The ground state minima are inequivalent, and give the splitting of the zero phonon line.

Finally we consider a (110) stress. The results here are most easily seen by recognising that we are only looking for effects *linear* in the applied stresses. To this order a (110) stress is equivalent to a sum of (111), $(\bar{1}11)$, (100) and (010) stresses. The first two split the excited state minima. The second two the ground state minima.

Table 3

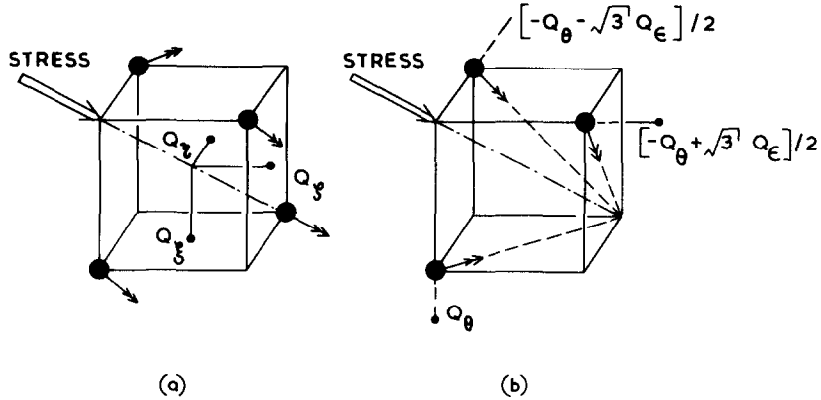|	(100)	(111)	(011)
Q_a/R	$P/(\sqrt{6}[c_{11}+2c_{12}])$	$P/(\sqrt{6}[c_{11}+2c_{12}])$	$P/(\sqrt{6}[c_{11}+2c_{12}])$
Q_θ/R	$P/(\sqrt{3}[c_{11}-c_{12}])$	·	$-P/(2\sqrt{3}[c_{11}-c_{12}])$
	·	$P/2c_{44}$	·
Q_T/R	·	·	$P/4c_{44}$

Fig. 3. The effect of a (111) stress on the minima of energy surfaces. The full circles
(●) represent the minima. In (a) the trigonal minima of the excited $^1T_2$ state are shown,
in (b) the tetragonal minima of the ^1E ground state.

The predicted splittings and relative intensities for a stress of given magnitude are given in Table 4. They are linear in the order terms tend to diverge. This means that the tetragonal and trigonal distortions of the excited state give very similar energies, and

Table 4. Here x,y,z label the tetragonally distorted states and 1,2,3,4 the (111), ($1\overline{11}$), ($\overline{1},1,\overline{1}$) and ($\overline{11},1$) trigonal states. The electric vector E has direction cosines (s/$\sqrt{2}$, $-s\sqrt{2}$,C) for the (110) σ case, where $s^2 + c^2 = 1$. Also we write

$$\delta_E = \tfrac{1}{2}I_{g\theta}Q_\theta(\sigma); \quad \delta_T = \tfrac{2}{3}I_{eT}[Q_\xi + Q_\eta + Q_\zeta]; \quad \delta_t = \tfrac{2}{3}I_{eT}Q_\zeta$$

| | | | θ ground state | | | ε ground state | |
Stress	Transition	Shift	σ intensity	π intensity	Shift	σ intensity	π intensity
100	$x \to$ 1,2,3,4	$2\delta_E$	4/3	16/3	$-2\delta_E$	4	0
	$y,z \to$ 1,2,3,4	$-\delta_E$	20/3	8/3	δ_E	4	8
111	$x,y,z \to 1$	$-3\delta_T$	3	0	$-3\delta_T$	3	0
	$x,y,z \to$ 2,3,4	δ_T	5	8	δ_T	5	8
110	$x,y \to$ 1,4	$-\dfrac{\delta_E}{2}-\delta_\zeta$	$\tfrac{1}{4}(4+14s^2)$	2/3	$-\dfrac{\delta_E}{2}-\delta_\zeta$	$4-2s^2$	2
	$x,y \to$ 2,3	$-\dfrac{\delta_E}{2}+\delta_\zeta$	$\tfrac{1}{4}(4-2s^2)$	6	$\dfrac{\delta_E}{2}+\delta_\zeta$	$4-2s^2$	2
	$z \to$ 1,4	$\delta_E-\delta_\zeta$	$\tfrac{1}{4}(8-8s^2)$	4/3	$-\delta_E-\delta_\zeta$	$4s^2$	0
	$z \to$ 2,3	$\delta_E+\delta_\zeta$	$\tfrac{1}{4}(8-4s^2)$	0	$-\delta_E+\delta_\zeta$	0	4

stresses; quadratic terms can be calculated, but a full second order calculation has not been attempted. A simple calculation of the second order terms shows one point of interest. If ΔE_{eE} and $\Delta E_{\theta T}$ are very close the second that only a very small perturbation is needed to change the order of the energies. There will be an apparently infinite response to a stress large enough to change the order of the minima.

The electric dipole selection rules affect the intensities of the lines. In Table 4 we give the energies and intensities of the different lines. The notation σ and π means that the electric field vector, $\mathbf{E}$, is parallel to the stress (π) or normal to it (σ). For the (110) direction there are two inequivalent σ polarisations, and we write the direction cosines of E as $c(0,0,1) + s(1,1,0)/\sqrt{2}$. The results are shown schematically in Fig. 4.
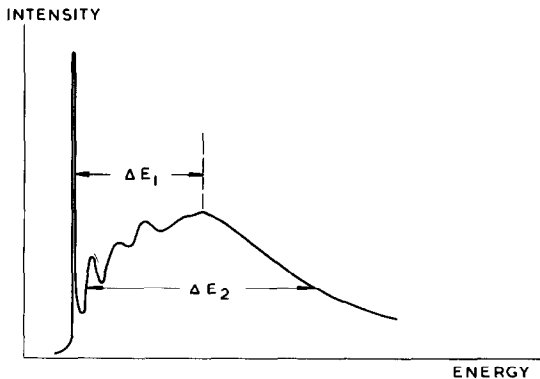
INTENSITY

Fig. 4. Schematic diagram of the GR1 band, defining ΔE_1 and ΔE_2.

6. COMPARISON WITH EXPERIMENT

Two centres observed in diamond have sometimes been identified with the neutral vacancy—the centre giving the optical GR1 band and the c system seen in spin resonance. Both are absent in unirradiated crystals and both are observed for all types of irradiation (e^-, n° or γ) with intensity proportional to the dose. Neither show any correlation with chemical impurities. These features suggest that the centres responsible are simple, intrinsic, lattice defects, and this is supported by other evidence. Under most conditions the 'c' system and GR1 band intensities are proportional, suggesting that the centres responsible are either identical or closely related (for example one being interstitial and the other a vacancy). Their annealing behaviour is different, however, so the centres are distinct. As the 'c' system centre becomes mobile at a lower temperature it is tempting to argue it is due to an interstitial rather than

a vacancy. The nature of the spin resonance from the 'c' system is consistent with either a neutral vacancy or a neutral interstitial; the ground state is diamagnetic with a tetragonal distortion, and the resonance is seen in a low-lying excited state with $S = 1$. The optical GR1 band has thus been associated, rather tenuously, with the neutral vacancy. This was supported by the calculations of[3] which predicted a transition energy of the right size. In this section we compare the properties of the band with our results in Sections 4 and 5. The data we use are measured band shapes, which give the Huang–Rhys factor, the polarisation of the luminescence and the stress splitting of the zero phonon line.

The work of Clark and Norris[15, 24] has shown that the luminescence from the GR1 band shows no polarisation at liquid nitrogen or liquid helium temperatures. This is consistent with our model, as emission from any trigonal excited state minimum can go with equal probability to any of the three tetragonally distorted ground states. This can be seen readily by symmetry arguments. The lack of polarisation is a very important result, as it is not predicted by some other models. For example, if the excited state had tetragonal minima ($\Delta E_{eE} > \Delta E_{eT}$) then polarisation would be expected. To get unpolarised luminescence either the Jahn–Teller effect must be negligible (which is inconsistent with the phonon structure of the GR1 band) or there must be sufficiently different symmetries in the states between which the transitions occur.

The second set of data come from Duncan's measurements of the band shape and F, the fraction of the intensity of the zero phonon line[14–16]. He measured F and found the Huang–Rhys factor to be

$$S_0 = 3 \cdot 57 \pm 0 \cdot 06$$

which is very close to our predicted 3·68. Measurement of F as a function of tempera-

ture yields an effective phonon energy of 0·099 eV, close to our $\hbar\omega_T = 0\cdot095$ eV. Duncan also measured the Stokes shift (ΔE_1 in Fig. 4) and band width (ΔE_2 in Fig. 4). These measurements have been supplemented by estimates of the moments of the band taken from a trace supplied by Dr. Duncan. The data are given in Table 2. The moments are not very accurate as other bands become important in the tail of the GR1 band, and it is particularly difficult to estimate M_1 and M_2 accurately. We see that experiment and theory are in acceptable accord for M_1 and M_2. The predicted values are rather larger than the measured ones, but this may be simply a result of difficulties of measurement. Also, the Jahn–Teller integrals (I_{eE}, I_{eT} and I_{gE}) are very sensitive to the wave functions chosen.

Two sets of stress splitting data are available[17, 18]. They are generally similar, but the diamonds used for the (110) and (111) stresses in[17] were too poor to be used here. The stress data are summarised in Fig. 5, where they are compared with the theory of the last section. This figure omits the small satellite lines of the GR1 zero phonon line. These satellites are present even for zero stress, but their origin is not fully understood. The comparison of the predicted and observed stress splittings leads to these conclusions. First, the (100) stress results are qualitatively similar. The polarisation measurements are only consistent with an $|\epsilon>$ ground state. Secondly, the (111) stress results are similar to those predicted only if one ignores one of the observed components. Thirdly, in both the (100) and (111) cases the relative intensities of the components do show deviations from the predictions although it is hard to measure intensities, so some of the discrepancies are experimental in origin. Fourthly, the (100) splitting which measures I_{gE}, is about 60 per cent of the observed value. This is quite good agreement. The (111) splitting, however, which measures I_{eT}, is found to be only 30 per cent of that predicted. The (110)
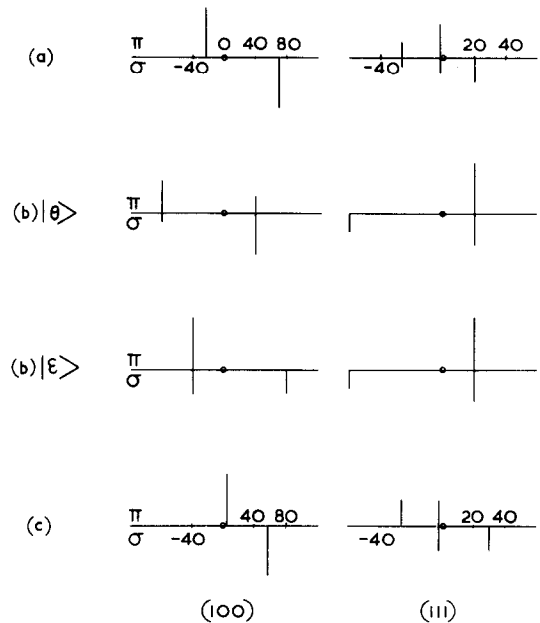

Fig. 5. The stress splitting of the zero phonon line of the GR1 band, measured experimentally, and the predictions for the neutral vacancy. The theoretical splittings in (b) are qualitative only, to make comparison of intensities easier. The experiments are those of[15] (case (a)) and [16] (case (c)).

results are too complicated to lead to any firm conclusions.

The differences in the magnitudes of the splittings from those predicted can be understood, in part, by recalling that we neglected local changes in force constant in Section 5, notably in equation (5.2). The remaining differences, the extra components (both satellite lines, and for example, the unexpected line seen in (111) stress) and the discrepancies in the relative intensities of the lines need a more sophisticated explanation.

Two explanations are apparent. The first is the possibility of a dynamic Jahn–Teller effect, either in the ground state or in the excited state, or possibly both. The barriers between the different minima in both states are at most of order 0·1 eV, and tunnelling cannot be ruled out. The interesting feature of a dynamic effect is that it can lead to a splitting of the ground and excited states. In

particular at low temperatures only the lowest of the ground states will be populated, so some of the lines should be frozen out. Exactly this behaviour is seen from the additional satellite lines, mentioned before. However it has not proved possible to correlate the observed transitions with the energy level schemes[25, 26] for the dynamic Jahn–Teller effect in E and T states. Nor is it obvious that the luminescence will be unpolarised if the excited state shows a dynamic effect. Fig. 6 shows the energy levels for various degrees of dynamic effect.

The second possibility is that the low-lying $^3T_1$ state may have a profound effect on the ground ^1E state. The ^1E state can, of course, only distort tetragonally in a static Jahn–Teller effect. However, when the separation of the ^1E and $^3T_1$ states is very small the electron-phonon interaction couples them in the presence of spin orbit coupling. The *coupled* states may have minima with lower symmetry than tetragonal, and this would affect the stress splitting and the selection rules. Further calculations are in progress on this point.

Conclusion

Our aim in this paper has been to answer two questions. First, what are the expected features of optical absorption by the neutral vancancy in diamond? Secondly, are the observed features of the GR1 band consistent with the properties of the neutral vacancy?

The energy levels of the neutral vacancy have been calculated previously. Our calculations have concentrated on the shape of the absorption band, rather than energy levels or oscillator strengths. We have assumed that the vacancy interacts with just six modes, corresponding to normal modes of its nearest neighbours. The relative magnitude of the frequencies of these modes have been estimated in a model in which only these nearest neighbours are allowed to move. The coupling of the electronic and nuclear motion has been estimated from an LCAO model in which the
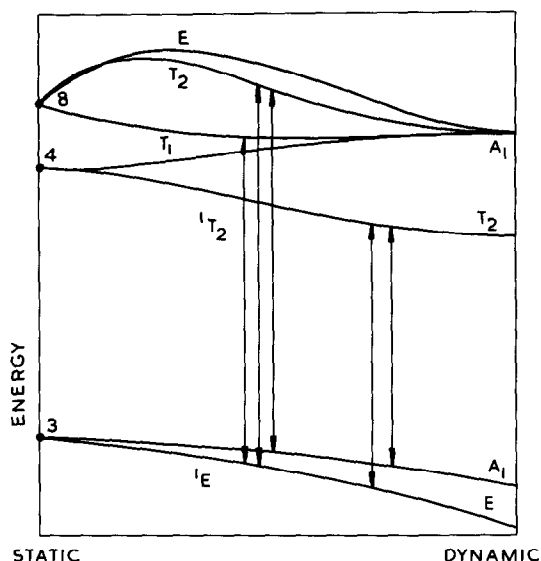

Fig. 6. The dynamic Jahn–Teller effect. The lowest vibronic states for ^1E $^1T_2$ are shown. In the static limit (discussed in this paper) the degeneracy of the levels is indicated. Allowed optical transitions are given; these need not be vertical in the diagram—the ground and excited states may be dynamic to different extents.

atomic orbitals move rigidly with the nuclei. In addition we have assumed that the Jahn–Teller effect is static. With these assumptions we calculated the Huang–Rhys factor, Stokes shift and band width. Further, we have predicted the absence of polarised luminescence and the character of the stress splitting of the zero phonon line.

It is harder to say if the GR1 band is associated with the vacancy. The present paper shows that the fractional intensity of the zero phonon line, the stokes shift, the band width and the absence of polarised luminescence are all consistent with this model. The stress experiments on the zero phonon line are harder to interpret, and the present theory and experiment show discrepancies. We can say, however, that if the stress results on the GR1 band are inconsistent with the neutral vacancy they are equally inconsistent with a neutral interstitial. The reason is that the low-lying energy levels of the two systems are (qualitatively) the same.

If the GR1 centre is one of these two fundamental defects then the current models must omit some essential features. Two possibilities were mentioned in Section 6—one that the Jahn–Teller effect should be dynamic, and the other than the low-lying $^3T_1$ level had a considerable effect on the properties of the ground ^1E state. Both these possibilities need further study.

REFERENCES

1. SWALIN R. A., *J. Phys. Chem. Solids* **18**, 290 (1961)
2. BENNEMANN K. H., *Phys. Rev.* **137**, A1497 (1965).
3. COULSON C. A. and KEARSLEY M. J., *Proc. R. Soc.* **241A**, 433 (1957).
4. YAMAGUCHI T., *J. phys. Soc. Japan* **17**, 1359 (1962).
5. YAMAGUCHI T., *J. phys. Soc. Japan* **18**, 368 (1963).
6. STONEHAM A. M., *Proc. phys. Soc.* **88**, 135 (1966).
7. LANNOO M., *Thèses de Troisieme Cycle*, Orsay (1966).
8. LIDIARD A. B. and STONEHAM A. M., *Science and Technology of Industrial diamonds*, Vol. 1, p. 1. Industrial Diamond Information Bureau, London (1967).
9. FRIEDEL J., LANDOO M., and LEMAN G., *Phys. Rev.* **164**, 1056 (1967).
10. HUANG K. and RHYS A., *Proc. R. Soc.* **A208**, 352 (1951).
11. MARKHAM J. J., *Rev. Mod. Phys.* **31**, 956 (1959).
12. PRYCE M. H. I.., *Phonons in Perfect Lattices and in Lattices with Point Imperfections.* (Edited by R. W. H. Stevenson), p. 403. Oliver and Boyd, London (1965).
13. LEMOS A. M. and MARKHAM J. J., *J. Phys. Chem Solids* **26**, 1837 (1965).
14. MITCHELL E. W. J., *Physical Properties of Diamond* (Edited by R. Berman), p. 394. Oxford University Press, London (1965).
15. MITCHELL E. W. J., *Science and Technology of Industrial Diamonds*, Vol. 1, p. 17. Industrial Diamond Information Bureau, London (1967).
16. DUNCAN I., Private communication.
17. RUNCIMAN W. A., *Proc. phys. Soc.* **86**, 629 (1965).
18. CROWTHER P. A., Private communication.
19. STURGE M. D., *Solid St. Phys.* **20**, 92 (1968).
20. LONGUET-HIGGINS H. C., *Adv. Spectrosc.* **2**, 429 (1961).
21. LAX M., *J. Chem. Phys.* **20**, 1752 (1952).
22. GOLD A. and KIEL T. H., *Phys. Status Solidi* **13**, 175 (1966).
23. HENRY C. E., SCHNATTERLY S. E. and SLICHTER, *Phys. Rev.* **137** A583 (1965).
24. CLARK C. D. and NORRIS C., *Diamond Conference*, Unpublished (1965).
25. O'BRIEN M. C. M., *Proc. R. Soc.* **A281**, 323 (1964).
26. CANER M. and ENGLMAN R., *J. chem. Phys.* **44**, 4054 (1966).

APPENDIX: THE NORMAL COORDINATES Θ_α

We label the neighbours of the vacancy A, B, C and D, where their coordinates are $(\bar{1}, 1, 1)$, $(1, \bar{1}, 1)$, $(1, 1, \bar{1})$ and $(1,1,1)$ respectively. Writing the x displacement of A as X_A and so on, the Q_α are given below.

$$Q_a = \frac{1}{\sqrt{12}}[\{-X_A + X_B + X_C - X_D\} + \{Y_A - Y_B + Y_C - Y_D\}$$

$$+ \{Z_A + Z_B - Z_C - Z_D\}]$$

$$Q_\theta = \frac{1}{\sqrt{24}}[2\{-X_A + X_B + X_C + X_D\}$$

$$- \{Y_A - Y_B + Y_C - Y_D\} - \{Z_A - Z_B - Z_C - Z_D\}]$$

$$Q_\epsilon = \frac{1}{\sqrt{8}}[\{Y_A - Y_B + Y_C - Y_D\} - \{Z_A + Z_B - Z_C - Z_D\}]$$

$$Q_\xi = \frac{1}{\sqrt{8}}[\{Y_A + Y_B - Y_C - Y_D\} + \{Z_A - Z_B + Z_C - Z_D\}]$$

$$Q_\eta = \frac{1}{\sqrt{8}}[\{X_A + X_B - X_C - X_D\} + \{-Z_A + Z_B + Z_C - Z_D\}]$$

$$Q_\zeta = \frac{1}{\sqrt{8}}[\{X_A - X_B + X_C - X_D\} + \{-Y_A + Y_B + Y_C - Y_D\}].$$